Applied Surface Science 270 (2013) 169–177

Contents lists available at SciVerse ScienceDirect

Applied Surface Science

journal homepage: www.elsevier.com/locate/apsusc

# $Au/TiO_2$ supported on ferritic stainless steel monoliths as CO oxidation catalysts

V.G. Milt[a,*], S. Ivanova[b], O. Sanz[b], M.I. Domínguez[b], A. Corrales[b], J.A. Odriozola[b], M.A. Centeno[b]

[a] Instituto de Investigaciones en Catálisis y Petroquímica - INCAPE (FIQ, UNL-CONICET), Santiago del Estero 2829, 3000 Santa Fe, Argentina
[b] Instituto de Ciencia de Materiales de Sevilla, Centro Mixto CSIC-Universidad de Sevilla, Av. Américo Vespucio 49, 41092 Sevilla, Spain

ARTICLE INFO

*Article history:*
Received 31 July 2012
Received in revised form
28 December 2012
Accepted 31 December 2012
Available online 7 January 2013

*Keywords:*
Structured catalysts
$Au/TiO_2$
CO oxidation
Metallic monoliths
Aluchrom YHf

ABSTRACT

Metallic supported structured catalysts were obtained by washcoating AluchromYHf monoliths with an $Au/TiO_2$ catalyst. The powder catalyst was synthesized by DAE (direct anionic exchange) method. Using this catalyst, a stable slurry was prepared and used to washcoat the monoliths. TEM and SEM studies revealed that gold nanoparticles in the $Au/TiO_2$ powder catalyst had an average diameter of 3–4 nm, but during the preparation of the structured catalyst, aggregate Au particles of the slurry reached diameters of 9 nm. Before coating, Aluchrom YHf monoliths were thermally treated to generate a homogeneous and well-adhered oxide rough surface layer, mainly composed of $\alpha$-$Al_2O_3$ whiskers, which favored the anchoring of the catalyst. The catalytic layer deposited was well attached and contained not only the $Au/TiO_2$ catalyst but also metallic oxides formed from stainless steel components that diffused through the oxide scale. The structural characterization was performed by XRD, XRF, TEM, SEM, GD-OES and $S_{BET}$.

The catalytic activity of the powder and structured catalysts was tested in the oxidation of the CO reaction. Catalysts demonstrated to be active at room temperature. After a first activation run, and in spite of their larger gold particle size, the catalytic activities of the structured catalysts overcame those of the powder catalyst. This improvement is probably due to the segregation of the transition metal oxides toward the surface oxide scale.



## 1. Introduction

The number of studies concerning the use of gold catalysts for different catalytic applications has grown exponentially in recent years [1–12]. These catalysts are particularly active toward oxidation reactions, specifically for CO removal at low temperature, such as total oxidation (TOX), CO preferential oxidation under $H_2$ streams (PROX) and water gas shift (WGS). The scientific and technological interest in these reactions has considerably increased since CO is one of the main atmospheric pollutants and constitutes the main poison of Pt electrodes in PEM fuel cells, which require $H_2$ streams free of CO (typically less than 10–50 ppm).

Besides, in gold catalysis $TiO_2$ is considered as an "active support" since it can provide active oxygen to gold particles, thus increasing the activity of gold catalysts toward the CO oxidation reaction [13].

On the other hand, interest in the use of structured catalysts and reactors, particularly monoliths and microreactors has increased in the last few years since they present considerable advantages if compared to powder catalysts (better energetic efficiency, high activity in relation to the catalyst active phase, safer working conditions, process intensification, etc.) [14–18]. Despite the extensive use of ceramic monoliths (mainly cordierite) in automotive exhaust catalysts, metallic monoliths are an interesting alternative to ceramic ones, especially in exothermic reactions since they present a series of comparative advantages such as higher mechanical strength, higher thermal conductivity, and lower thermal inertia and lightness. Under certain circumstances, these advantages could compensate their higher costs. The main problem with preparing the metallic monolith catalytic devices lies in the low adhesion between the metallic substrate and the catalytic coating. However, this problem is often overcome by the use of Al-containing ferritic stainless steels treated at high temperature; at this temperature they segregate scales that improve the adherence of the catalytic coating to the surface [19]. These scales are mainly composed of $\alpha$-$Al_2O_3$ in the form of needle-like whisker structures, although doping elements present in the stainless steel (such as Y, Zr and Ti) tend to become incorporated into them and modify their protective properties [20].

The direct deposition of the gold ethylenediamine complex on modified carbon fibers reported by Bulushev et al. [21] and the two-step preparation of $Au/TiO_2$/carbon-carbon composites, reported by Hammer et al. [22], were employed as structured reactors for low temperature CO oxidation. However the nature of the metallic monoliths and the response of the metal to chemical treatments do not allow the use of either the direct adsorption or the deposition precipitation methods for the preparation of gold catalysts. The deposition of powder gold catalysts over metallic structures then

* Corresponding author. Fax: +54 342 4536861.
*E-mail address:* vmilt@fiq.unl.edu.ar (V.G. Milt).

0169-4332/$ – see front matter © 2013 Published by Elsevier B.V.
http://dx.doi.org/10.1016/j.apsusc.2012.12.159

has to be done by washcoating. $Au/Al_2O_3$, $Au/CeO_2$, $Au/CeO_2/Al_2O_3$, Au/pillarized bentonites and Au/cryptomelane solids have been successfully deposited on stainless steels monoliths [17,19,23–25]. However, catalyst deposition can result in modifications of the catalyst through the interaction between the coating and the metal oxidation scale. These modifications can affect the activity of the catalyst and depend on the atmosphere and reaction conditions, with the alteration of the catalytic features upon reaction time being possible [24].

To the best of our knowledge, no studies on the preparation of metallic monoliths washcoated with $Au/TiO_2$ catalysts have been published, whereas the use of ceramic substrates or carbon-carbon composites has been already reported [22,26]. In this vein, the objectives of this work are to determine if the deposition of the powder $Au/TiO_2$ catalyst over metallic surfaces is feasible in order to apply these systems as structured catalysts for processes where either $TiO_2$ or $Au/TiO_2$ have proved to be very active (i.e. photocatalytic reaction, CO oxidation, etc.) and to study the influence of the metallic substrate on the activity of the catalyst. The correlations between structure and activity behavior of the powder and the structured catalyst are also established.

## 2. Experimental

### 2.1. Powder $Au/TiO_2$ catalyst

The powder $Au/TiO_2$ catalyst (denoted as "$Au/TiO_2$") was prepared by the direct anionic exchange method (DAE), as reported elsewhere [27]. An aqueous solution of $HAuCl_4$ of concentration $5.7 \times 10^{-4}$ mol $L^{-1}$ was stirred and heated up to 70 °C during 30 min, after which $TiO_2$ (Degussa P25) was added. The amount of $TiO_2$ added was calculated in order to obtain a final Au loading of 2 wt.%. The slurry was stirred at 70 °C during 20 min. Then, at room temperature, $NH_3$ was added under continuous stirring and after 20 min, the obtained solid was filtered, dried overnight at 120 °C and finally calcined at 300 °C during 4 h.

### 2.2. Structured support (metallic monolith)

Commercial Aluchrom YHf ferritic chromium steel sheets (50 μm thick) were used as raw material. The weight chemical composition of the employed steel is: 20% Cr and 5.5% Al (Fe balance). Ni (0–0.3%), C (0–0.05%), Mn (0–0.5%), Si (0–0.5%), Zr (0–0.07%), Y (0–0.1%) and Hf (0–0.1%) could also be present. The sheets were washed with water and soap and then put in a vessel with acetone in an ultrasonic bath for 30 min. Monoliths were prepared by rolling around a spindle alternate flat and corrugated sheets to obtain a cylindrical monolith of 25 mm in height and 15 mm in diameter (cell density = 155 cell $cm^{-2}$). The prepared monoliths were cleaned again with acetone in ultrasound for 30 min.

The monoliths were thermally treated to generate a rough adherent oxide layer for a better anchoring of the subsequent catalytic film. This treatment consisted in heating the monoliths in a furnace at 900 °C during 22 h at a heating rate of 10 °C $min^{-1}$. As described elsewhere [28], this treatment produces the adequate oxide thickness that makes this layer thermally and mechanically stable. The thermally treated monoliths were denoted as M(900).

Following the same procedure, 2 × 2 cm Aluchrom YHf plates of different thickness (50 and 600 μm) were prepared. The thermally treated plates were denoted as P(900). The thicker plates were necessary to analyze the composition of the structured catalysts in depth by GD-OES.

### 2.3. Structured catalyst: deposition of the $Au/TiO_2$ powder catalyst onto the monoliths

The catalyst deposition was carried out by washcoating using a slurry containing the $Au/TiO_2$ catalyst. The slurry was prepared using water as solvent, with 2 wt.% of PVA (polyvinylalcohol), 5 wt.% of the $Au/TiO_2$ catalyst powder and 5 wt.% of $Al_2O_3$ colloidal suspension (Nyacol, 20 wt.%). Considering the total content in solids, the slurry contained 16.7 wt.% of alumina. Taking into account the IEP of the catalyst (6.67), the pH of the slurry was adjusted to 4 by adding a $HNO_3$ solution (2 M). At this pH, the catalyst particles were positively charged and the stability of the slurry was guaranteed. The viscosity of the slurry was 3.2 cP. The thermally pretreated monoliths were immersed into the prepared slurry at a constant speed of 3 cm $min^{-1}$, maintained during 1 min and then withdrawn at the same constant speed. The excess of slurry in the monolith channels was removed by centrifugation at 400 rpm for 10 min. After the catalytic coating deposition, monoliths were dried in a stove at 140 °C. In order to increase the amount of the catalyst loading, the above described procedure was repeated several times, weighing after each one. Two batches of monoliths with 5 and 10 cycles were prepared. After all the immersion steps, monoliths were calcined at 300 °C for 4 h at 10 °C $min^{-1}$ and denoted as $Au/TiO_2(5)/M$ and $Au/TiO_2(10)/M$, respectively.

Following the same procedure, structured catalysts deposited on thermally treated plaques (see Section 2.2) were prepared repeating the immersion step into the slurry suspension from 1 to 10 cycles, the only difference being the absence of the centrifugation step. Finally, the systems were calcined at 300 °C for 4 h at 10 °C $min^{-1}$ and the catalysts were denoted as $Au/TiO_2(5)/P$ and $Au/TiO_2(10)/P$, respectively.

It should be noted that the slurry contains not only the powder $Au/TiO_2$ catalyst but also some additives like PVA and Nyacol used to achieve the required rheological properties, namely desired viscosity and stability of the suspension. In order to check how these additives affected the characteristics of the catalyst, the slurry remaining after the coatings was dried in a stove at 140 °C overnight and then it was milled and calcined at 300 °C for 4 h at 10 °C $min^{-1}$. This solid was labeled as $Au/TiO_2 + Al_2O_3$.

### 2.4. Characterization

X-ray diffraction analyses (XRD) were obtained with a Siemens D500 diffractometer, using Cu Kα radiation (λ = 1.5404 Å) from $2\theta = 10°$ to $2\theta = 80°$ at a scan rate of 1° $min^{-1}$.

The gold content of the powder samples was determined by X-ray fluorescence spectrometry (XRF) in a Siemens SRS 3000 sequential spectrophotometer with a rhodium tube as the source radiation. XRF measurements were performed onto pressed pellets (10 wt.% sample in wax).

The textural properties were determined by $N_2$ adsorption at -196 °C in a Micromeritics ASAP 2010 equipment. Before the analysis, samples were degassed for 2 h at 150 °C in a vacuum. Conventional cells were used for the powder catalysts and in the case of monoliths, they were put in a homemade cell that allowed analyzing the complete monolith [19]. The degassing pretreatment was the same as that used for the powder catalyst and in the case of the structured catalysts, BET surface area values were expressed per gram of deposited catalyst.

The morphology of the samples was analyzed by SEM (scanning electron microscopy) using a JEOL 5400 instrument and TEM (Transmission electron microscopy) using a Philips CM 200 microscope operating at 200 kV. In the case of the structured catalysts, the plaques were analyzed.

The adherence of the catalytic layer to the monolith was evaluated by the ultrasonic method [29]. The monoliths immersed in

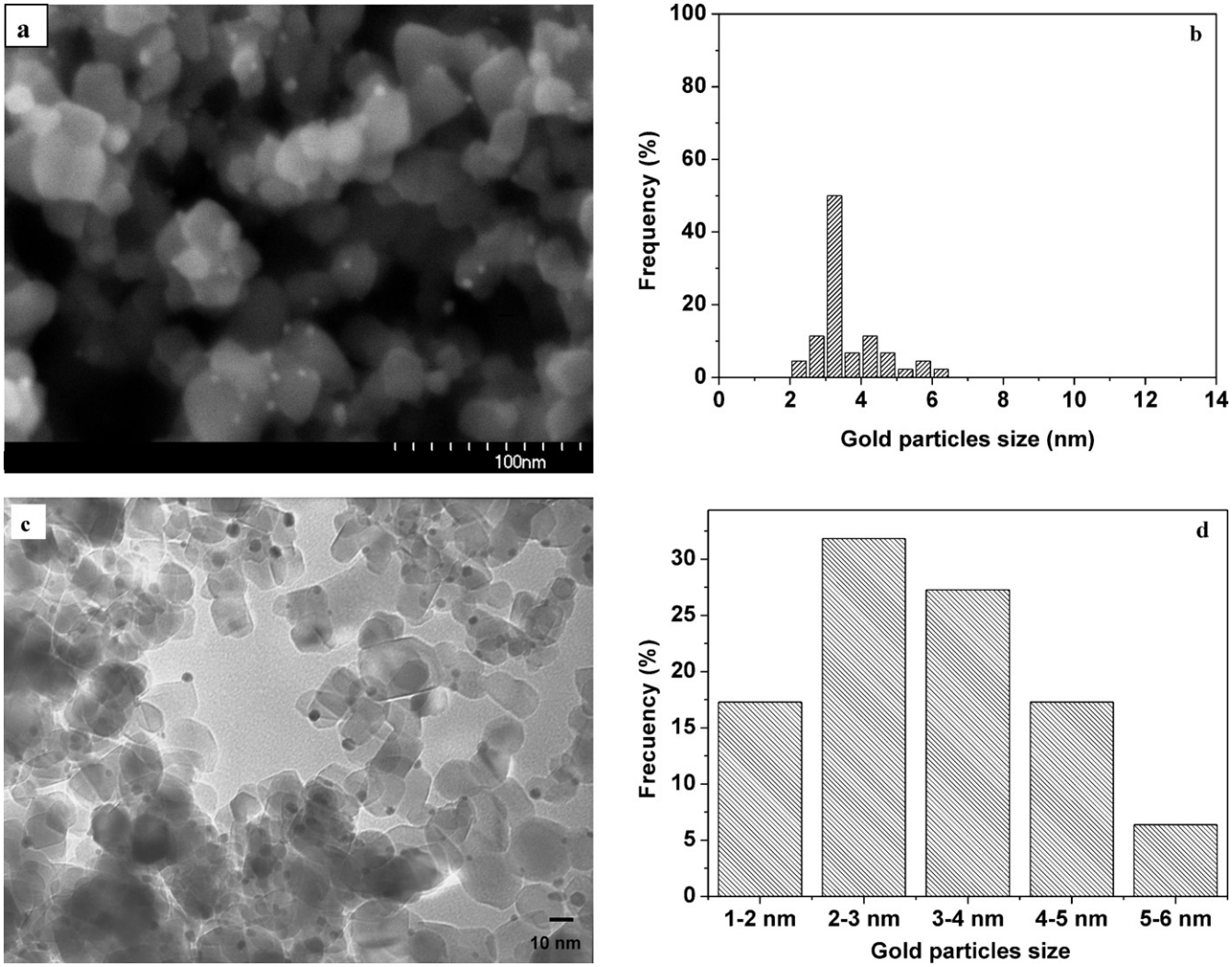


**Fig. 1.** (a) SEM image of the powder $Au/TiO_2$ catalyst; (b) gold particle size distribution in the $Au/TiO_2$ powder catalyst obtained from SEM results; (c) TEM image of the powder $Au/TiO_2$ catalyst and (d) gold particle size distribution in the $Au/TiO_2$ powder catalyst obtained from TEM results.

ethyl ether were submitted to an ultrasonic treatment in a Cole Palmer ultrasonic bath (47 kHz and 30 W) for 30 min at room temperature, which was controlled by water circulation. After that, the sample was dried at 80 °C overnight and calcined at 300 °C for 4 h. The weight loss was determined by the difference in mass of the samples before and after the ultrasonic test, both after drying at 80 °C and calcination at 300 °C. Results are presented in terms of adherence, which is defined as the retained quantity of coating on the monolith, expressed in percentage. In the case of the calcined monoliths (without catalyst), the stability test was performed in order to study the stability of the oxide scale formed after calcination of the ferritic stainless steel support.

The isoelectric point (IEP) of the powder catalyst was determined in a ZETAMASTER equipment. The slurry viscosity was measured in a Brookfield RVDVIII viscometer. Roughness was measured with a Mitutoyo SJ-201P surface roughness tester on catalysts supported on plaques.

In-depth compositional analysis of the catalytic layer deposited on plaques was determined by Glow Discharge Optical Emission Spectroscopy (GD-OES) experiments using a LECO GDS 750A spectrometer. The GD-OES analyses were performed with a Grimm lamp in the DC mode at 700 V using a constant power of 14 W. In order to ensure average macroscopic information of the analyzed plaques, a 4 mm-diameter area was analyzed in all cases.

### 2.5. Catalytic activity

The catalytic oxidation of CO was carried out in a conventional continuous flow U-shaped glass reactor operating at atmospheric pressure. The inlet and outlet gas compositions were analyzed with a Balzers Thermostar mass spectrometer. The light-off curves for CO oxidation were obtained with a gas mixture of 3.4% CO and 21% $O_2$ (He balance), with a total gas flow of 42 $cm^3\ min^{-1}$. The reactant stream was passed through the reactor during 45 min at room temperature and then the temperature was increased at 10 °C $min^{-1}$ up to 300 °C and kept in this value for 1 h. No activity was observed under these conditions with the empty reactor (blank test). The catalysts were activated in situ at 300 °C for 60 min under the reaction conditions. In the light-off curves, the activation runs was indicated as "1st". Then, always under reactant stream, the temperature was decreased from 300 °C to room temperature and, after stabilization; the temperature was raised again to 300 °C with a heating ramp of 10 °C $min^{-1}$ and kept at this temperature for 1 h. The corresponding light-off curve was denoted as "2nd". In the case of the powder catalyst, a total weight of 80 mg of catalyst with particle size below

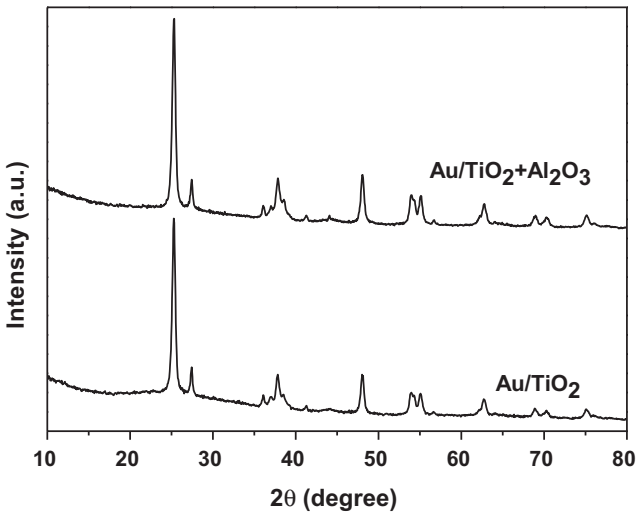


**Fig. 2.** XRD patterns of the powder catalysts.

100 μm was used, the weight hourly space velocity (WHSV) of the catalytic test being 31500 mL g(cat)$^{-1}$ h$^{-1}$.

## 3. Results and discussion

### 3.1. Powder catalyst

The SEM picture of the powder catalyst (Au/$TiO_2$, Fig. 1a) shows that gold particles are homogeneously distributed into the $TiO_2$ matrix. The particle size distribution is schematized in Fig. 1b, where it can be noticed that 50% of the gold particles are 3.2 nm in diameter. The average particle size indicates that the mean diameter of gold nanoparticles is 4 nm, the standard deviation being 1 nm. It is expected that gold particles of smaller size, which cannot be detected by SEM, could also be present. The TEM technique allowed us to obtain better particle size distribution (Fig. 1c). Fig. 1d shows the corresponding gold nanoparticle size distribution, the average size being 3.1 nm, lower than that obtained using SEM data.

No diffraction signals corresponding to metallic gold (2$\theta$: 38.3, 44.6, 64.6 or 77.55°) are observed in the XRD pattern of the Au/$TiO_2$ catalyst (Fig. 2), although the gold content as measured by XRF was 1.93 wt.% (Table 1), which emphasizes the small dimension of gold particles. All diffraction lines observed in Fig. 2 for the Au/$TiO_2$ catalyst correspond to anatase (JCPDS 71-1167) and rutile (JCPDS 76-0319) phases of $TiO_2$, according to the P25 $TiO_2$ used for the preparation of the powder catalysts. On the other hand, the XRD pattern of the Au/$TiO_2$ + $Al_2O_3$ solid is very similar to that of the Au/$TiO_2$ catalyst, although a low intensity reflection at 2$\theta$ = 44.6 is observed which highlights the existence of larger polycrystalline gold particles. After subtraction of the XRD pattern of the titania support the other gold diffractions emerged (not shown). The size of the gold crystallites calculated from the broadening of these reflection peaks and applying the Scherrer equations is 10 nm.

The SEM picture of the Au/$TiO_2$ + $Al_2O_3$ solid (Fig. 3a) shows that gold particles remained homogeneously distributed although they had a higher particle size than gold particles in the Au/$TiO_2$ catalyst. This means that, after all the immersion steps of monoliths and plaques into the slurry, Au particles aggregate to some extent, the average particle size of gold particles in the Au/$TiO_2$ + $Al_2O_3$ solid being 9 nm (Fig. 3b), which agrees with the XRD data.

**Table 1**
Catalysts composition.

| Sample | wt.% $Al_2O_3$ | wt.% $TiO_2$ | wt.% Au | Au/$TiO_2$ ratio (wt./wt.) |
|---|---|---|---|---|
| Au/$TiO_2$ | – | 98.07 | 1.93 | 0.020 |
| Au/$TiO_2$ + $Al_2O_3$ | 2.25 | 95.40 | 2.34 | 0.025 |

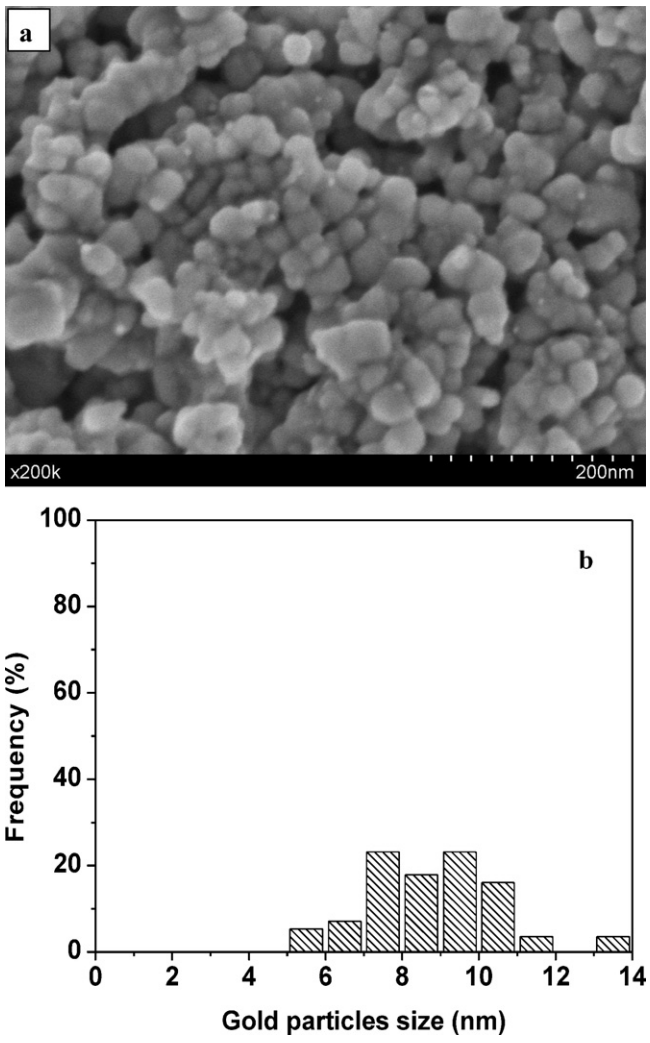


**Fig. 3.** (a) SEM image of the powder Au/$TiO_2$ + $Al_2O_3$ catalyst and (b) gold particles size distribution in the Au/$TiO_2$ + $Al_2O_3$ powder catalyst.

The BET surface area of the Au/$TiO_2$ catalyst was 52 m$^2$ g$^{-1}$ whereas in the case of the Au/$TiO_2$ + $Al_2O_3$ solid it was 56 m$^2$ g$^{-1}$. The slightly higher value observed for the Au/$TiO_2$ + $Al_2O_3$ solid is due to the presence of colloidal $Al_2O_3$ that contributes to the BET surface area of Au/$TiO_2$, since the powder specific surface area obtained after drying and calcination at 300 °C of the colloidal alumina suspension is 192 m$^2$ g$^{-1}$. Considering the BET surface area of the Au/$TiO_2$ catalyst and that corresponding to the colloidal $Al_2O_3$, the content in alumina of the slurry after the coating process can be estimated in 3 wt.%, in good agreement with the chemical composition obtained by XRF analysis (Table 1). The alumina content in the post- deposition slurry is well below its initial value (16.7 wt.%), pointing to a preferential deposition of $Al_2O_3$ over the metallic substrates, in agreement with the chemical compatibility of the colloidal alumina with the oxide scale (mainly composed of α-$Al_2O_3$) generated after the ferritic steel thermal treatment.

### 3.2. Structured catalyst

Fig. 4 shows that the catalyst weight incorporated to the monoliths is almost linear with the number of immersion steps. The average catalyst weight gained per monolith after 5 immersions

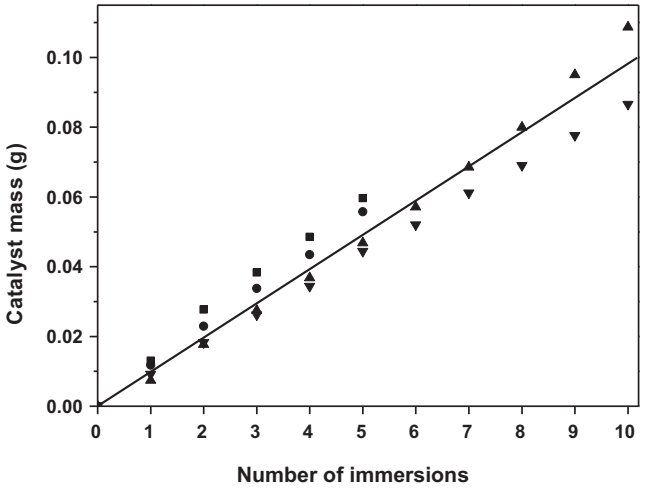


**Fig. 4.** Catalyst loaded to different pieces of monoliths after each immersion step: Rectangles and circles correspond to two batches of $Au/TiO_2(5)/M$ preparations and up and down triangles, to two batches of $Au/TiO_2(10)/M$ preparations.

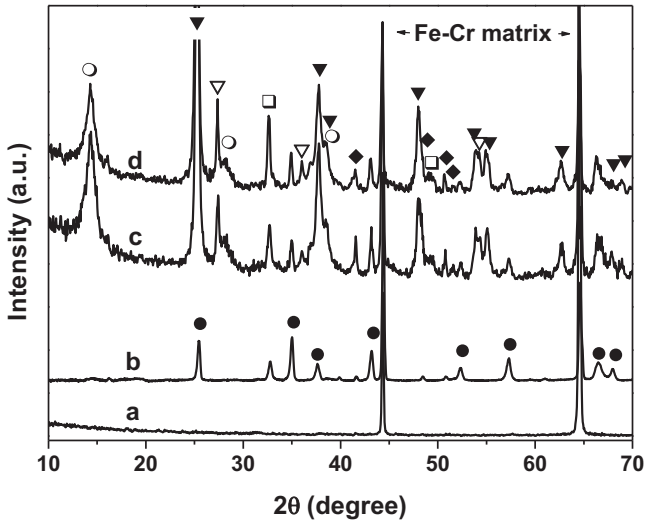


**Fig. 5.** XRD patterns of the structured catalysts. ● $\alpha$-$Al_2O_3$, ○ boehmite, ▼ $TiO_2$ anatase, ▽ $TiO_2$ rutile, □ $Mn_2O_3$, ♦ $M_{23}C_6$. (a) Aluchrom plate, (b) Aluchrom plate calcined at 900 °C for 22 h (P900), (c) $Au/TiO_2(5)/P$ and (d) $Au/TiO_2(10)/P$.

is 57.7 mg and after 10 immersions, 96.8 mg. This indicates that after each immersion cycle, approximately 10 mg of catalyst are loaded onto the monolith walls. From these values, and considering the geometric area of the monoliths (325 $cm^2$), the surface loading onto the structured catalyst can be estimated in 0.18 mg $cm^{-2}$ and 0.30 mg $cm^{-2}$ for $Au/TiO_2(5)/M$ and $Au/TiO_2(10)/M$, respectively.

As the surface area of the oxidized metallic monolith is hardly measurable, (below 1 $m^2$ $g^{-1}$) the measured surface area and porosity of the monolith correspond directly to the catalytic layer. The specific surface areas of the structured catalysts were 85.5 $m^2$ $g^{-1}$ for the $Au/TiO_2(5)/M$ and 94.4 $m^2$ $g^{-1}$ for the $Au/TiO_2(10)/M$ catalyst (referred to the mass of deposited coating). These values are higher than those obtained for the powder solid, caused by the important contribution of the alumina additive, used in the preparation of the slurry. As explained before, taking into account the BET specific surface areas of the colloidal $Al_2O_3$ and the $Au/TiO_2$ powder catalyst and assuming that no important changes in the textural properties of both solids occur, the relative proportion of $Al_2O_3$ to $Au/TiO_2$ can be estimated. In the case of $Au/TiO_2(5)/M$, the coating is composed of 24% $Al_2O_3$ and 76% $Au/TiO_2$ and for $Au/TiO_2(10)/M$, the composition of the coating is 30% $Al_2O_3$ and 70% $Au/TiO_2$, in both cases the coating is enriched in alumina in comparison to the initial alumina content in the slurry (16.7 wt.%). The latter also agrees with the observed deficiency in $Al_2O_3$ content into the post-deposition slurry (3 wt.%).

Taking into account the BET surface area values and the weight increment of the monoliths both after calcination and after the catalyst deposition, the thickness of the different oxide layers could be estimated. For the calculus, the density of the $Al_2O_3$ was taken as 4.0 g $cm^{-3}$ and that of $TiO_2$, 4.2 g $cm^{-3}$ [30]. The calculated thicknesses were 0.5 μm for the oxide layer of the calcined Aluchrom monolith, 1.1 μm for the catalytic layer of $Au/TiO_2(5)/M$ and 1.7 μm for $Au/TiO_2(10)/M$.

The commercial support (Aluchrom YHf) exhibits two intense XRD reflection lines at 44.4° and 64.5° that correspond to the Fe-Cr matrix with a BCC structure (Fig. 5a, [31]). After calcination at 900 °C for 22 h, diffraction peaks characteristics of $\alpha$-$Al_2O_3$ (corundum, JCPDS 75-1862), metal carbides (typically $Cr_{23}C_6$, JCPDS 71-0552) and manganese oxide ($Mn_2O_3$, JCPDS78-0390) become visible (Fig. 5b).

Reflections of the stainless steel support still appear in the XRD pattern of the structured catalyst (Fig. 5c and d), together with a signal corresponding to anatase (JCPDS 71-1167), rutile (JCPDS 76-0319) and boehmite (JCPDS 21-1307). As expected, the higher the number of coatings, the lower the intensity of the metal support signals and the higher the intensity of the catalyst reflections. However, the complexity of the XRD diagrams prevents the detection of gold reflections.

The chemical composition of the structured catalysts from the metallic surface of the Aluchrom YHf plaque and through the catalytic coating was analyzed by GD-OES. The thickness of the oxide scale generated after Aluchrom YHf calcination at 900 °C for 22 h (P900) was estimated in about 0.9 μm (Fig. 6a), where two different areas can be distinguished. The most external layer (<0.7 μm) is enriched in Si and slightly in C and Mn in relation to the bulk composition (Fig. 6b). Silicon entering in the composition of $SiO_2$ and manganese is present in its oxide form ($Mn_2O_3$), as confirmed by XRD. Finally, as XRD reveals, carbon appears as $M_{23}C_6$-type carbides. In the internal layer, the aluminum oxide is the main species, having its maximum at 0.8 μm of depth and gradually tending to Al bulk concentration of the ferritic steel support as considering inner depths (Fig. 6a). However, composition in the outer atomic layers is not reliable because there is insufficient time for the sputtering to reach a steady state, since a preferential sputtering (removal of some elements more readily than others) normally occurs [32].

For the $Au/TiO_2(5)/P$ catalyst (Fig. 7a), the thickness of the layer is about 1.4 μm. Three zones can be identified in the depth profile. The more external layer, of about 0.1 μm in thickness, is enriched not only in carbon and silicium but also in manganese and nickel (Fig. 7b). The presence of Mn and Ni indicates the additional modification of the oxide scale composition with the coating process [24]. Below this region, there is a 1 μm layer enriched in titanium that corresponds to the catalytic coating. Therefore, there is no clear interface between the catalytic coating and the external oxide layer; in addition, some titanium also migrates to the external layer. This phenomenon was observed before in the case of austenitic stainless steel coated with $CeO_2$ [24]. The third layer is mainly composed of alumina (Fig. 7a). It is interesting to note that the intensity of the Al signal on the external surface of the $Au/TiO_2(5)/P$ catalyst is higher than that exhibited for the bare calcined Aluchrom support (46 wt.% vs. 16 wt.% at the maximum value, see Figs. 6a and 7a). This could be directly related to the addition of colloidal $Al_2O_3$ to the slurry and its subsequent preferential deposition on the calcined Aluchrom plate, where Al is preferentially segregated after thermal treatment at 900 °C.

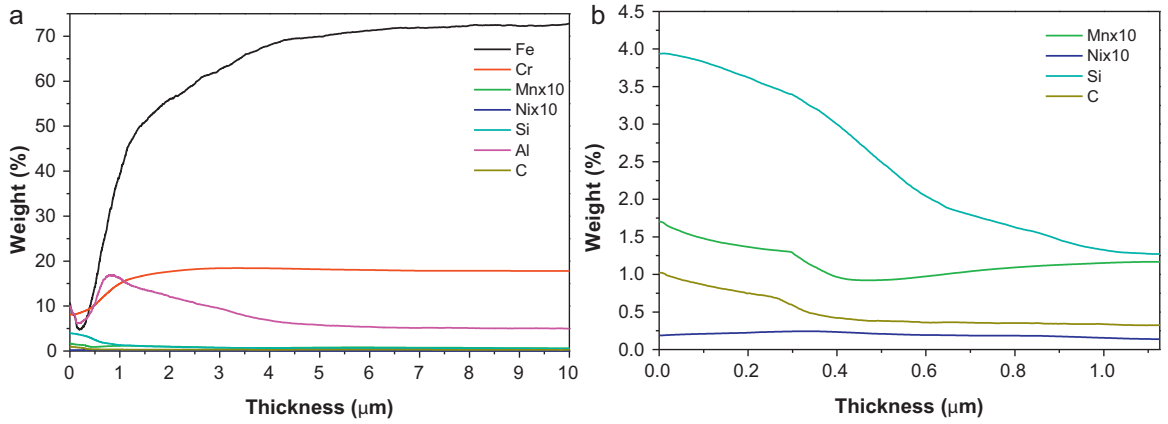


**Fig. 6.** In depth compositional analysis of the scale formed on the Aluchrom YHf plate after calcination at 900 °C for 22 h (GD-OES): (a) Profiles of the main ferritic stainless steel components and (b) profiles of some components of the oxide scale.

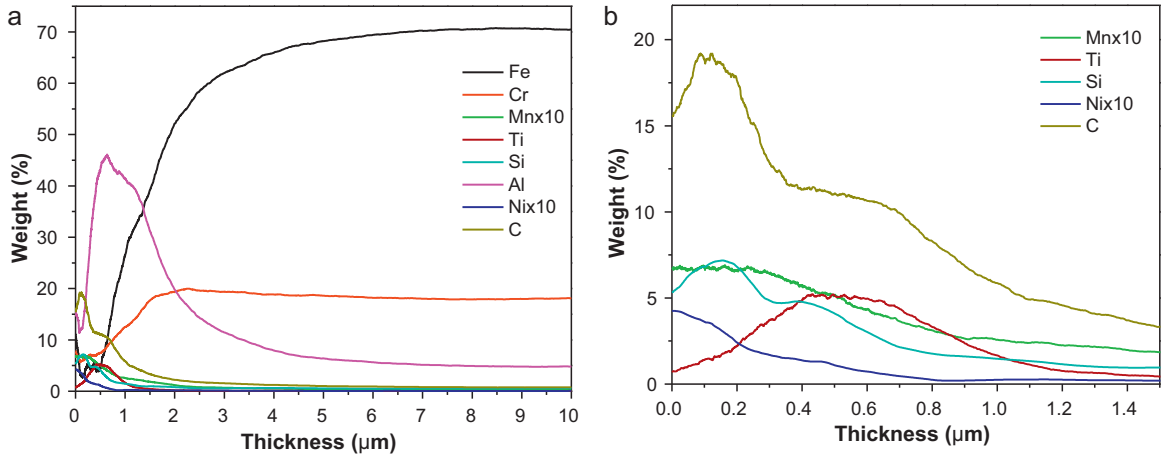


**Fig. 7.** In depth compositional analysis of Au/$TiO_2$(5)/P (GD-OES). (a) Profiles of the main ferritic stainless steel components and (b) profiles of some components of the oxide scale.

GD-OES results on Au/$TiO_2$(10)/P (Fig. 8a) reveal the segregation of the same elements as observed for Au/$TiO_2$(5)/P, with an increase of the thickness of the catalytic layer (2.5 μm). The titania distribution curve in the catalytic layer shifts to a higher depth, broadens and increases in value (Fig. 8b), which agrees with the increase of the surface loading of catalyst.

Thickness values experimentally obtained are higher than the calculated ones, probably because the estimation based on the surface area and the layer density underestimates the thickness of the layer, due to the decreased porosity of the coating, as reported by Rebrov et al. [33].

Another outstanding point from GD-OES is that, even after the incorporation of the Au/$TiO_2$ catalyst to the Aluchrom calcined plates, the presence of elements that constitute the ferritic support (Fe, Al, Si and Cr) is also observed on the external surface (outer 2 μm). This is more pronounced after the catalytic

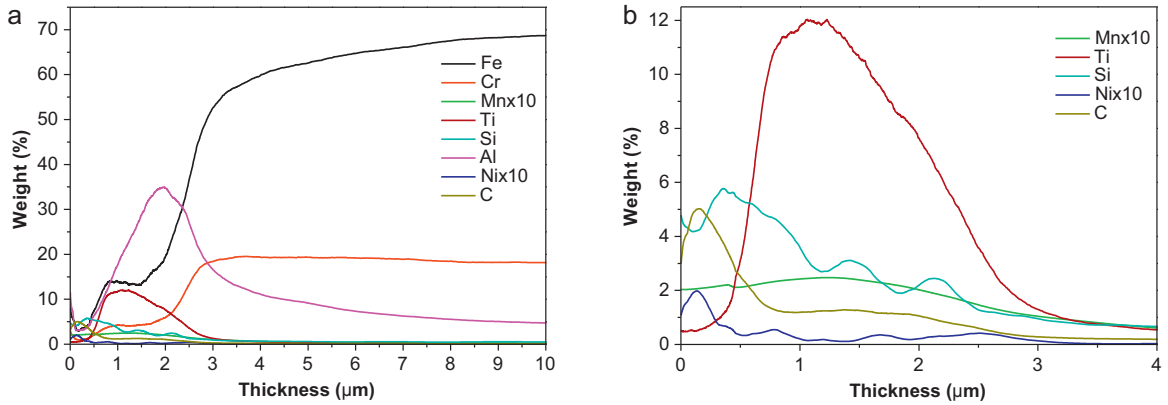


**Fig. 8.** In depth compositional analysis of Au/$TiO_2$(10)/P (GD-OES). (a) Profiles of the main ferritic stainless steel components and (b) profiles of some components of the oxide scale.

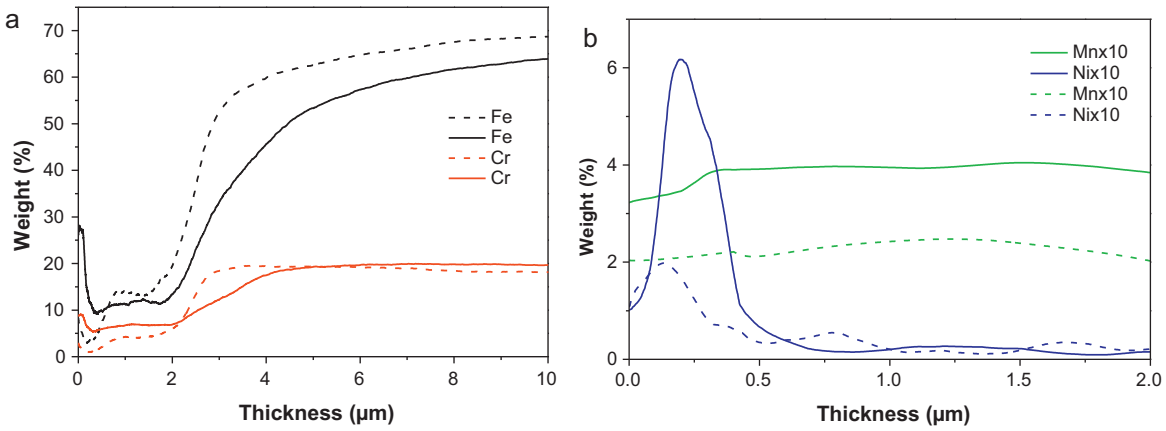


**Fig. 9.** Comparison of the in-depth compositional analysis of Au/$TiO_2$(10)/P (GD-OES) before (dashed lines) and after (solid lines) CO oxidation runs: (a) Profiles of the main ferritic stainless steel components and (b) profiles of some components of the oxide scale.

evaluation and implies the mobility of the constituent elements of the ferritic support along the catalytic coating (Fig. 9).

As it is observed in Table 2, the calcination of the plates notably increases the surface roughness due to the formation of the oxide layer that favors the anchoring of the catalyst, as previously analyzed. The addition of the catalytic layer through the immersion of the calcined plate into the slurry suspension five times (Au/$TiO_2$(5)/P catalyst) slightly modifies the surface roughness, whereas a notable increase in roughness up to 0.59 μm is observed after ten coatings (Au/$TiO_2$(10)/P catalyst).

The oxide scale generated after the calcination of the plate (mainly composed of $Al_2O_3$) exhibits an excellent adherence to the monolith walls since it presents no weight loss after the adherence test. In a similar way, the adherence of the catalytic coating to the metallic substrate is very good, both monoliths, Au/$TiO_2$(5)/M and Au/$TiO_2$(10)/M, retaining 89 and 98 wt.% of the weight of catalyst initially deposited, respectively.

### 3.3. Catalytic oxidation test

The light-off curves (Fig. 10) indicate that the Au/$TiO_2$ catalyst oxidizes CO at room temperature (CO conversion = 6.5%), being $T_{50\%}$ = 143 °C. The powder catalyst exhibits slight higher activity after its first run ($T_{50\%}$ = 131 °C), reaching 100% CO conversion at 300 °C.

For the structured catalysts, practically no activity is observed for the monolith calcined at 900 °C. In the first run, both Au/$TiO_2$(5)/M and Au/$TiO_2$(10)/M monoliths present a lower activity than the powder catalyst, the CO conversion at room temperature being lower than 2% and the $T_{50\%}$ = 219 °C and 209 °C, respectively. This behavior could be related to the higher average size of gold particles determined by SEM (9 nm) for the Au/$TiO_2$ + $Al_2O_3$ slurry, compared to the 4 nm determined for the Au/$TiO_2$ catalyst. However, once activated, the monoliths show a noticeable increase in activity, greatly surpassing the powder catalyst results. At room temperature the conversion is 26.5% for Au/$TiO_2$(5)/M and 38% for Au/$TiO_2$(10)/M. The 100% CO conversion is observed at 187 °C and 146 °C, respectively.

**Table 2**
Surface roughness.

| Sample | Roughness (μm) |
|---|---|
| Aluchrom YHf | 0.14 |
| P(900) | 0.39 |
| Au/$TiO_2$(5)/P | 0.41 |
| Au/$TiO_2$(10)/P | 0.59 |

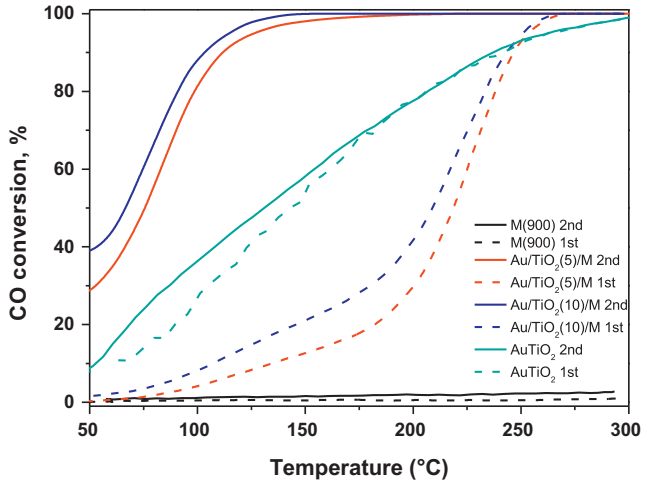


**Fig. 10.** CO oxidation activity of the powder and monolithic catalysts. First runs indicated by dashed lines and second runs by solid lines.

The specific reaction rates of the considered catalysts at 80 °C and their turnover frequency values (TOF) (defined as the number of moles of CO converted per mole of surface gold atom per second) in the two reaction cycles measured are shown in Table 3. For the calculation of the TOF, gold dispersions of 37 and 16% were considered for the Au/$TiO_2$ powder and the monolithic devices, respectively. These dispersions were based on the assumption of the calculated average gold particle sizes from SEM and XRD results (3 and 9 nm) and a mathematical model for cuboctahedral particles [34].

Our Au/$TiO_2$ powder catalyst presents a specific reaction rate of $1.9 \times 10^{-4}$ $mol_{CO}$ $s^{-1}$ $g_{Au}{}^{-1}$, and a TOF of 0.10 in the second run. These values are lower than those normally reported in other studies for Au/$TiO_2$ [13,35], although similar to those described by Kozlov et al. [36].

In the first reaction cycle, both monolithic devices present lower specific reaction rates and TOF values than those of the powder

**Table 3**
Reaction rates and turnover frequencies calculated at 80 °C in the 1st and 2nd ligth-off CO oxidation reactions on the considered catalytic devices.

| Sample | Reaction rate ($\times 10^4$) ($mol_{CO}$ $s^{-1}$ $g_{Au}{}^{-1}$) | | TOF ($s^{-1}$) | |
|---|---|---|---|---|
| | 1st | 2nd | 1st | 2nd |
| Au/$TiO_2$ | 1.1 | 1.9 | 0.06 | 0.10 |
| Au/$TiO_2$(5)/M | 0.1 | 7.0 | 0.03 | 0.86 |
| Au/$TiO_2$(10)/M | 0.4 | 5.4 | 0.04 | 0.67 |

sample. However, in their second cycle, these values significantly increase, reaching TOF values 7–9 times higher. An increase of the reaction rate with the number of cycles was also reported by Hammer et al. [22] for the $Au/TiO_2$ carbon-carbon composite structure catalyst, which they assigned to the changes on the catalyst surface as a function of the type of the applied heating - Joule effect. However, in external heating mode the activity of the samples basically depends on the atmosphere of activation, heating rate and final temperature, as reported by Park and Lee [37]. However, when the conditions of activation are the same, some other factors have to be taken in consideration. In order to elucidate the reason for the activation of these systems, it is convenient to go back to GD-OES results. The calcination of the Aluchrom plate generates an oxide scale (mainly composed of $Al_2O_3$) and after the catalytic test, Fe and Cr oxides are segregated toward the oxide scale. However, as seen in Fig. 10, these chromium or iron oxides practically do not contribute by themselves to the catalytic properties shown by the monoliths.

On the other hand, the GD-OES study also demonstrates that, after the CO oxidation reaction, the scale thickness increases (from 2.5 to 3 μm for $Au/TiO_2(10)/P$) and the composition changes (Fig. 9). Ni and Mn appear more exposed and thus, the observed activation of the structured gold catalysts could be related to the segregation of Ni and Mn oxides which, together with the surface presence of chromium and iron oxides, could help to activate the gold species or even catalyze by themselves the CO oxidation due to their recognized oxidation and redox properties. All these factors lead to the increase in the specific activity of the exposed gold particles, which becomes more evident in the $Au/TiO_2(5)/M$ devices, where the thinner catalytic layer deposited onto the metallic walls favors the diffusion and transport phenomena of reactants [24]. Bulushev et al. [21] also found that the addition of iron oxide was beneficial for the Au dispersion and catalytic activity. In this context and as found in the literature [24], the migration of iron species to the surface cannot be fully discarded. A detailed operando DRIFTS study is currently under way in order to clarify this point.

## 4. Conclusions

The applied washcoating procedure allowed us to deposit a powder of Au nanoparticles supported on $TiO_2$ over ferritic stainless steel monoliths. The catalytic layer resulted well adhered to the metallic support, which was previously calcined in order to increase the roughness of the surface in order to favor the anchoring of the catalyst. The formed $Al_2O_3$ whiskers at the outer surface increase the chemical affinity of the monolith walls to the colloidal alumina used as additive during the washcoating process. Increasing the number of immersions of the monoliths into the slurry results in increasing thicknesses of the catalytic layer (to ca. 2.5 μm thick after 10 immersions). The subsequent calcination of the structured catalysts causes the diffusion of elements constituent of the metallic monolith into the catalytic layer, resulting in a scale mainly composed of Al, Ti, Au, Ni and Mn. The scale composition somehow differs from that of $Au/TiO_2(5)/P$ and $Au/TiO_2(10)/P$, which indicates that not only the number of immersions of the monoliths into the slurry affects the scale composition but also the drying and calcination steps.

The $Au/TiO_2$ powder catalyst, in which gold particles are of nanometric size, resulted active toward the CO oxidation reaction. Nevertheless, the structured catalysts demonstrated to be more active in the studied reaction than the powder catalyst since after calcinations, and moreover under reaction conditions, some elements (mainly Ni and Mn) constituting the metallic monolith diffuse into the catalytic layer, enhancing the catalytic features of $Au/TiO_2$ catalyst for the oxidation of CO.

## Acknowledgements

The financial support for this work has been obtained from Junta de Andalucía (TEP106) and Ministerio Español de Ciencia e Innovación (ENE2009-14522-C05-01) cofinanced by FEDER funds from European Union. S. Ivanova acknowledges the same Ministry for her Ramón y Cajal contract. V. Milt thanks CONICET that financed her external fellowship in the Instituto de Ciencia de Materiales, Centro Mixto CSIC-Universidad de Sevilla, España. Evonik/Quimidroga, S.A. is kindly acknowledged for supplying the Titania P25.

## References

[1] G.C. Bond, C. Louis, D.T. Thompson, in: G.H. Hutchings (Ed.), Catalysis by Gold, Imperial College Press, London, 2006.
[2] G.C. Bond, D.T. Thompson, Catalysis Reviews: Science and Engineering 41 (3–4) (1999) 319–388.
[3] M. Lamallem, R., Cousin, R., Thomas, S., Siffert, F. Aïssi, A. Aboukaïs, C.R. Chimie 12 (6-7) (2009) 772-778.
[4] G.C. Bond, D.T. Thompson, Gold Bulletin 33 (2000) 41–50.
[5] O.H. Laguna, F. Romero Sarria, M.A. Centeno, J.A. Odriozola, Journal of Catalysis 276 (2) (2010) 360–370.
[6] Y. Denkwitz, B. Schumacher, G. Kučerová, R.J. Behm, Journal of Catalysis 267 (2009) 78–88.
[7] M.A. Centeno, M. Paulis, M. Montes, J.A. Odriozola, Applied Catalysis B 61 (2005) 177–183.
[8] L.M. Molina, B. Hammer, Applied Catalysis A 291 (2005) 21–31.
[9] O.H. Laguna, M.A. Centeno, G. Arzamendi, L.M. Gandía, F. Romero-Sarria, J.A. Odriozola, Catalysis Today 157 (2010) 155–159.
[10] V.P. Santos, S.A.C. Carabineiro, P.B. Tavares, M.F.R. Pereira, J.J.M. Órfão, J.L. Figueiredo, Applied Catalysis B 99 (2010) 198–205.
[11] M. Kotobuki, R. Leppelt, D.A. Hansgen, D. Widmann, R.J. Behm, Journal of Catalysis 264 (2009) 67–76.
[12] M.I. Domínguez, F. Romero-Sarria, M.A. Centeno, J.A. Odriozola, Applied Catalysis B 87 (2009) 245–251.
[13] M.M. Schubert, S. Hackemberg, A.C. van Veen, M. Muhler, V. Plzak, R.J. Behm, Journal of Catalysis 197 (2001) 113–122.
[14] B.P. Barbero, L. Costa-Almeida, O. Sanz, M.R. Morales, L.E. Cadus, M. Montes, Chemical Engineering Journal 139 (2008) 430–435.
[15] P. Ávila, M. Montes, E. Miró, Chemical Engineering Journal 109 (2005) 11–36.
[16] M.I. Domínguez, M. Sánchez, M.A. Centeno, M. Montes, J.A. Odriozola, Journal of Molecular Catalysis A: Chemical 277 (1–2) (2007) 145–154.
[17] L.M. Martínez, M.I. Domínguez, N. Sanabria, W.Y. Hernández, S. Moreno, R. Molina, J.A. Odriozola, M.A. Centeno, Applied Catalysis A 364 (1–2) (2009) 166–173.
[18] L.C. Almeida, F.J. Echave, O. Sanz, M.A. Centeno, J.A. Odriozola, M. Montes, Studies in Surface Science and Catalysis 175 (2010) 25–33.
[19] L.M. Martínez, O. Sanz, M.I. Domínguez, M.A. Centeno, J.A. Odriozola, Chemical Engneering Journal 148 (2009) 191–200.
[20] L. Niewolak, D. Naumenko, E. Wessel, L. Singheiser, W.J. Quadakkers, Materials Characterization 55 (2005) 320–331.
[21] D.A. Bulushev, L. Kiwi-Minsker, I. Yuranov, E.I. Suvorova, Ph A. Buffat, A. Renken, Journal of Catalysis 210 (2002) 149–159.
[22] N. Hammer, S. Zarubova, I. Kvande, D. Chen, M. Ronning, Gold Bulletin 40 (2007) 234–239.
[23] L.M. Martínez, D.M. Frías, M.A. Centeno, A. Paúl, M. Montes, J.A. Odriozola, Chemical Engineering Journal 136 (2008) 390–397.
[24] L.M. Martínez, O. Sanz, M.A. Centeno, J.A. Odriozola, Chemical Engineering Journal 162 (2010) 1082–1090.
[25] L.M. Martínez, F. Romero-Sarria, W.Y. Hernández, M.A. Centeno, J.A. Odriozola, Applied Catalysis A 423–424 (2012) 137–145.
[26] F. Moreau, G.C. Bond, R. Hughes, J.A. Moulijn, M. Makee, K. Krishna, B.A.A. Silberova, Gold Bulletin 40 (2008) 291–294.
[27] S. Ivanova, C. Petit, V. Pitchon, Applied Catalysis A 267 (2004) 191–201.
[28] L.C. Almeida, O. González, O. Sanz, A. Paul, M.A. Centeno, J.A. Odriozola, M. Montes, Studies in Surface Science and Catalysis 167 (2007) 79–84.
[29] S. Yasaki, Y., Yoshino, K. Ohkubo, US Patent 5,208,206 (1993).
[30] Handbook of Chemistry and Physics, David R. Lide, (Editor-in-Chief), 84th Edition, 2003-2004. CRC Press.
[31] M. Stanislowski, E. Wessel, T. Markus, L. Singheiser, W.J. Quadakkers, Solid State Ionics 179 (2008) 2406–2415.
[32] R. Payling, in: R. Payling, D. Jones, A. Bengtson (Eds.), Glow discharge optical emission spectrometry, John Wiley & Sons, New York, 1997, p. 715.

[33] E.V. Rebrov, G.B.F. Seijger, H.P.A. Calis, M.H.J.M. de Croon, C.M. van den Bleek, J.C. Schouten, Applied Catalysis A 206 (2001) 125–143.
[34] S. Ivanova, V. Pitchon, C. Petit, Journal of Molecular Catalysis A: Chemical 256 (2006) 278–283.
[35] S. Ivanova, V. Pitchon, C. Petit, V. Caps, ChemCatChem 2 (5) (2010) 556–563.
[36] A.I. Kozlov, A.P. Kozlova, H. Liu, Y. Iwasawa, Applied Catalysis A 182 (1999) 9–28.
[37] E.D. Park, J.S. Lee, Journal of Catalysis 186 (1999) 1–11.